

Simple models suffice for the single dot quantum shuttle

A Donarini^{†‡}, T Novotný^{*+}, and A-P Jauho[†]

[†] NanoDTU, MIC – Department of Micro and Nanotechnology, Technical University of Denmark (DTU), Building 345 East, DK – 2800 Kongens Lyngby, Denmark

[‡] Institut I - Theoretische Physik Universität Regensburg D-93040 Regensburg, Germany

^{*} Nano-Science Center, University of Copenhagen, Universitetsparken 5, DK – 2100 Copenhagen Ø, Denmark

⁺ Department of Electronic Structures, Faculty of Mathematics and Physics, Charles University, Ke Karlovu 5, 121 16 Prague, Czech Republic

Abstract. A quantum shuttle is an archetypical nanoelectromechanical device, where the mechanical degree of freedom is quantized. Using a full-scale numerical solution of the generalized master equation describing the shuttle, we have recently shown [Novotný *et al.*, Phys. Rev. Lett. **92**, 248302 (2004)] that for certain limits of the shuttle parameters one can distinguish three distinct charge transport mechanisms: (i) an incoherent tunneling regime, (ii) a shuttling regime, where the charge transport is synchronous with the mechanical motion, and (iii) a coexistence regime, where the device switches between the tunneling and shuttling regimes. While a study of the cross-over between these three regimes requires the full numerics, we show here that by identifying the appropriate time-scales it is possible to derive vastly simpler equations for each of the three regimes. The simplified equations allow a clear physical interpretation, are easily solved, and are in good agreement with the full numerics in their respective domains of validity.

1. Introduction

A generic example of a nanoelectromechanical (NEMS) device is given by the *charge shuttle* (originally proposed by Gorelik *et al.* [1]): a movable single-electron device, working in the Coulomb blockade regime, which can exhibit regular charge transport, where one electron within each mechanical oscillation cycle is transported from the source to the drain – see Figure 1 for a schematic illustration (see also Ref.[2], which contains an illustrative computer animation).

The device shown in Fig. 1 can exhibit a number of different charge transport mechanisms, to be discussed below, and transitions between the various regimes can be induced by varying a control parameter, such as the applied bias, or the mechanical damping. Since its introduction, the charge shuttle has inspired a large number of theoretical papers (see, *e.g.*, Refs. [3, 4, 5, 6, 7, 8, 9, 10, 11]). To the best of our knowledge, a clear-cut experimental demonstration of a shuttling transition is not yet available, though significant progress has been made, such as the *driven* shuttle of Erbe *et al.* [12], or the nanopillars studied by Scheible and Blick [13]. In the present paper, we study the quantum shuttle, *i.e.* a device where also the mechanical motion needs to be quantized (the physical condition for this to happen is $\lambda \simeq x_{zp}$, where

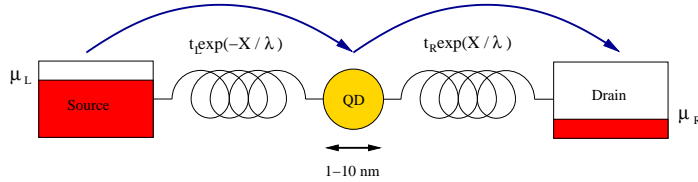


Figure 1. Schematic representation of the single-dot shuttle: electrons tunnel from the left lead at chemical potential (μ_L) to the quantum dot and eventually to the right lead at lower chemical potential μ_R . The position dependent tunneling amplitudes are indicated. X is the displacement from the equilibrium position. The springs represent the harmonic potential in which the central dot can move.

λ is the tunneling length describing the exponential decay of the wave-functions into vacuum, and x_{zp} is the quantum-mechanical zero-point amplitude). In contrast to many of the earlier theoretical papers on quantum shuttles [3, 4, 7, 8], where extensive numerical calculations were employed, the main aim here is to develop simplified models which allow significant analytic progress, and hence lead to a transparent physical interpretation. From the previous numerical studies we know that there are (at least) three well-defined transport regimes for a quantum nanomechanical device: (i) the tunneling regime, (ii) the shuttle regime, and (iii) the coexistence regime. As we show in subsequent sections, each of these regimes is characterized by certain inequalities governing the various time-scales, and a systematic exploitation of these inequalities allows us then to develop the aforementioned simplified models. In all three cases we will compare the predictions of the simplified models to the ones obtained with the full numerics. While in most cases the comparison is very satisfactory, we do not always observe quantitative agreement; these discrepancies are analyzed and directions for future work are indicated.

The paper is organized as follows. In Sections 2, 3 and 4 we briefly introduce the microscopic model for the quantum shuttle, introduce the Klein-Kramers equations for the Wigner functions, and summarize the phenomenology extracted from previous numerical studies, respectively. Section 5 contains the main results of this paper, *i.e.*, the derivations and analysis of the simplified models for the three transport regimes. We end the paper with a short conclusion of the main results.

2. The Single-Dot Quantum Shuttle

The Single-Dot Quantum Shuttle (SDQS) consists of a movable quantum dot (QD) suspended between source and drain leads (see Fig. 1). The center of mass of the QD is confined to a potential that, at least for small displacements from its equilibrium position, can be considered harmonic. Due to its small geometric size, the QD has a very small capacitance and thus a charging energy that may exceed the thermal energy $k_B T$ (approaching room temperature in the most recent realizations [13]). For this reason we assume that only one excess electron can occupy the device (Coulomb blockade) and we describe the electronic state of the central dot as a two-level system (empty/charged). Electrons can tunnel between leads and dot with tunneling amplitudes which depend exponentially on the position of the central island due to the decreasing/increasing overlapping of the electronic wave functions. The Hamiltonian

of the model reads:

$$H = H_{\text{sys}} + H_{\text{leads}} + H_{\text{bath}} + H_{\text{tun}} + H_{\text{int}} \quad (1)$$

where

$$\begin{aligned} H_{\text{sys}} &= \frac{\hat{p}^2}{2m} + \frac{1}{2}m\omega^2\hat{x}^2 + (\varepsilon_1 - e\mathcal{E}\hat{x})c_1^\dagger c_1 \\ H_{\text{leads}} &= \sum_k (\varepsilon_{l_k} c_{l_k}^\dagger c_{l_k} + \varepsilon_{r_k} c_{r_k}^\dagger c_{r_k}) \\ H_{\text{tun}} &= \sum_k [T_l(\hat{x})c_{l_k}^\dagger c_1 + T_r(\hat{x})c_{r_k}^\dagger c_1] + h.c. \\ H_{\text{bath}} + H_{\text{int}} &= \text{generic heat bath} \end{aligned} \quad (2)$$

The hat over the position and momentum (\hat{x}, \hat{p}) of the dot indicates that they are operators since the mechanical degree of freedom is quantized. Using the language of quantum optics we call the movable grain alone the *system*. This is then coupled to two electric *baths* (the leads) and a generic heat bath. The system is described by a single electronic level of energy ε_1 and a harmonic oscillator of mass m and frequency ω . When the dot is charged the electrostatic force ($e\mathcal{E}$) acts on the grain and gives the *electrical influence* on the mechanical dynamics. The electric field \mathcal{E} is generated by the voltage drop between left and right lead. In our model, though, it is kept as an external parameter, also in view of the fact that we will always assume the potential drop to be much larger than any other energy scale of the system (with the only exception of the charging energy of the dot).

The leads are Fermi seas kept at two different chemical potentials (μ_L and μ_R) by the external applied voltage ($\Delta V = (\mu_L - \mu_R)/e$) and all the energy levels of the system lie well inside the bias window. The oscillator is immersed into a dissipative environment that we model as a collection of bosons coupled to the oscillator by a weak bilinear interaction:

$$\begin{aligned} H_{\text{bath}} &= \sum_{\mathbf{q}} \hbar\omega_{\mathbf{q}} d_{\mathbf{q}}^\dagger d_{\mathbf{q}} \\ H_{\text{int}} &= \sum_{\mathbf{q}} \hbar g \sqrt{\frac{2m\omega}{\hbar}} \hat{x} (d_{\mathbf{q}} + d_{\mathbf{q}}^\dagger) \end{aligned} \quad (3)$$

where the operator $d_{\mathbf{q}}^\dagger$ creates a bath boson with wave number \mathbf{q} . The damping rate is given by:

$$\gamma(\omega) = 2\pi g^2 D(\omega) \quad (4)$$

where $D(\omega)$ is the density of states for the bosonic bath at the frequency of the system oscillator. A bath that generates a frequency independent γ is called Ohmic.

The coupling to the electric baths is introduced with the tunneling Hamiltonian H_{tun} . The tunneling amplitudes $T_l(\hat{x})$ and $T_r(\hat{x})$ depend exponentially on the position operator \hat{x} and represent the *mechanical feedback* on the electrical dynamics:

$$T_{l,r}(\hat{x}) = t_{l,r} \exp(\mp \hat{x}/\lambda) \quad (5)$$

where λ is the tunneling length. The tunneling rates from and to the leads ($\bar{\Gamma}_{L,R}$) can be expressed in terms of the amplitudes:

$$\bar{\Gamma}_{L,R} = \langle \Gamma_{L,R}(\hat{x}) \rangle = \left\langle \frac{2\pi}{\hbar} D_{L,R} \exp\left(\mp \frac{2\hat{x}}{\lambda}\right) |t_{l,r}|^2 \right\rangle \quad (6)$$

where $D_{L,R}$ are the densities of states of the left and right lead respectively and the average is taken with respect to the quantum state of the oscillator.

The model has three relevant time scales: the period of the oscillator $2\pi/\omega$, the inverse of the damping rate $1/\gamma$ and the average injection/ejection time $1/\bar{\Gamma}_{L,R}$. It is possible also to identify three important length scales: the zero point uncertainty $x_{zp} = \sqrt{\frac{\hbar}{2m\omega}}$, the tunneling length λ and the displaced oscillator equilibrium position $d = \frac{e\mathcal{E}}{m\omega^2}$. The ratios between the time scales and the ratios between length scales distinguish the different operating regimes of the SDQS.

3. Klein-Kramers Equation

The shuttle dynamics has an appealing simple classical interpretation: the name ‘‘shuttle’’ suggests the idea of sequential and periodical loading, mechanical transport and unloading of electrons between a source and a drain lead. Motivated by the possibility of observing signatures of quantum dynamics of the mechanical degree of freedom for a nanoscale shuttle, we decided, following the suggestion of Armour and MacKinnon [3], to explore a system with a quantized oscillator. We express our results in terms of the Wigner function because in this way we can simultaneously keep the intuitive phase-space picture and handle the quantum-classical correspondence [4].

The phase space of the shuttle device is spanned by the triplet charge – position – momentum. Correspondingly, the Wigner function is constructed from the reduced density matrix σ_{ii} ($i = 0, 1$ indicates the empty and charged states respectively):

$$W_{ii}(q, p, t) = \frac{1}{2\pi\hbar} \int_{-\infty}^{+\infty} d\xi \left\langle q - \frac{\xi}{2} \left| \sigma_{ii}(t) \right| q + \frac{\xi}{2} \right\rangle \exp\left(\frac{ip\xi}{\hbar}\right) \quad (7)$$

where the reduced density matrix σ is defined as the trace over the mechanical and thermal baths of the full density matrix:

$$\sigma = \text{Tr}_B\{\rho\} \quad (8)$$

The dynamics of the shuttle device is then completely described by the equation of motion for the Wigner distribution [5, 14]:

$$\begin{aligned} \frac{\partial W_{00}}{\partial t} &= \left[m\omega^2 q \frac{\partial}{\partial p} - \frac{p}{m} \frac{\partial}{\partial q} + \gamma \frac{\partial}{\partial p} p + \gamma m \hbar \omega \left(n_B + \frac{1}{2} \right) \frac{\partial^2}{\partial p^2} \right] W_{00} \\ &\quad + \Gamma_R e^{2q/l} W_{11} - \Gamma_L e^{-2q/l} \sum_{n=0}^{\infty} \frac{(-1)^n}{(2n)!} \left(\frac{\hbar}{l} \right)^{2n} \frac{\partial^{2n} W_{00}}{\partial p^{2n}} \\ \frac{\partial W_{11}}{\partial t} &= \left[m\omega^2 (q - d) \frac{\partial}{\partial p} - \frac{p}{m} \frac{\partial}{\partial q} + \gamma \frac{\partial}{\partial p} p + \gamma m \hbar \omega \left(n_B + \frac{1}{2} \right) \frac{\partial^2}{\partial p^2} \right] W_{11} \\ &\quad + \Gamma_L e^{-2q/l} W_{00} - \Gamma_R e^{2q/l} \sum_{n=0}^{\infty} \frac{(-1)^n}{(2n)!} \left(\frac{\hbar}{l} \right)^{2n} \frac{\partial^{2n} W_{11}}{\partial p^{2n}} \end{aligned} \quad (9)$$

where (q, p) are the position and momentum coordinates of the mechanical phase space and n_B is the Bose distribution calculated at the natural frequency of the harmonic oscillator. Only the diagonal charge states enter the Klein-Kramers equations (9): the off-diagonal charge states vanish given the incoherence of the leads and are thus excluded from the dynamics.

We distinguish in Eqs. (9) contributions of different physical origin: the coherent terms that govern the dynamics of the (shifted) harmonic oscillator, the dissipative terms proportional to the mechanical damping constant γ and, finally the driving terms proportional to the bare tunneling rates $\Gamma_{L,R}$.

The ability of the formalism to treat the quantum-classical correspondence is explicit in Eqs. (9): given a length, a mass, and a time scale for the system we can rescale the phase space coordinates and an expansion in \hbar/S_{sys} will appear where S_{sys} is the typical action of the system. Classical systems have a large action $S_{\text{sys}} \gg \hbar$ and only the first term ($\hbar/S_{\text{sys}} \rightarrow 0$) in the expansion is relevant. In the opposite limit $S_{\text{sys}} \approx \hbar$ the full expansion should be considered.

4. Phenomenology

The stationary solution of the Klein-Kramers equations for the Wigner distributions (9) describes the average long time behavior of the shuttling device. Information about the different long time operating regimes can be extracted from the distribution itself or from the experimentally accessible stationary current and zero frequency current noise.

The mechanical damping rate γ is the control parameter of our analysis. At high damping rates the total Wigner distribution is concentrated around the origin of the phase space and represents the harmonic oscillator in its ground state. While reducing the mechanical damping a ring develops and, after a short coexistence, the central “dot” eventually disappears (Figure 2). The ring is the noisy representation of the low damping limit cycle trajectory (shuttling) that develops from the high damping equilibrium position (tunneling). Equilibrium and limit cycle dynamics coexist in the intermediate damping bistable configuration where the system randomly switches between tunneling and shuttling regimes. The charge resolved Wigner distributions W_{00} and W_{11} also reveal the charge-position (momentum) correlation typical of the shuttling regime: for negative displacements and positive momentum (*i.e.* leaving the source lead) the dot is prevalently charged while it is empty for positive displacements and negative momentum (coming from the drain lead).

Also the stationary current and the current noise (expressed in terms of the Fano factor) show distinctive features for the different operating regimes. At high damping rates the shuttling device behaves essentially like the familiar double-barrier system since the dot is (almost) static and far from both electrodes. The current is determined essentially by the bare tunneling rates $\Gamma_{L,R}$ and the Fano factor differs only slightly from the values found for resonant tunneling devices ($F = 1/2$ for a symmetric device). At low damping rates the current saturates at one electron per mechanical cycle (corresponding to current $I/e\omega = 1/2\pi$) since the electrons are shuttled one by one from the source to the drain lead by the oscillating dot while the extremely sub-poissonian Fano factor reveals the deterministic character of this electron transport regime. The fingerprint of the coexistence regime, at intermediate damping rates, is a substantial enhancement of the Fano factor. The current interpolates smoothly between the shuttling and tunneling limiting values (Figure 3).

The cross-over damping rate is determined by the effective tunneling rates of the electrons. We get the following physical picture: every time an electron jumps on the movable grain the grain is subject to the electrostatic force $e\mathcal{E}$ that accelerates it towards the drain lead. Energy is pumped into the mechanical system and the dot starts to oscillate. If the damping is high compared to the tunneling rates the

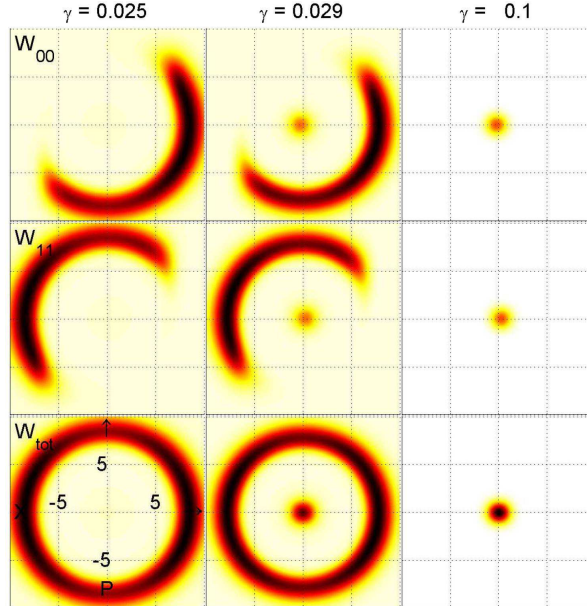


Figure 2. Charge resolved Wigner function distributions for different mechanical damping rates (horizontal axis: coordinate in units of $x_0 = \sqrt{\hbar/m\omega}$; vertical axis: momentum in \hbar/x_0). The rows represent from top to bottom the empty (W_{00}), charged (W_{11}) and total ($W_{\text{tot}} = W_{00} + W_{11}$) Wigner distribution respectively. The columns represent from left to right the shuttling ($\gamma = 0.025 \omega$), coexistence ($\gamma = 0.029 \omega$) and tunneling regime ($\gamma = 0.1 \omega$) respectively. The Figure is partially reproduced from [7].

oscillator dissipates this energy into the environment before the next tunneling event: on average the dot remains in its ground state. On the other hand, for very small damping the relaxation time of the oscillator is long and multiple “forcing events” occur before the relaxation takes place. This continuously drives the oscillator away from equilibrium and a stationary state is reached only when the energy pumped per cycle into the system is dissipated during the same cycle in the environment.

5. Simplified models

We qualitatively described in the previous section three possible operating regimes for shuttle-devices. The specific separation of time scales allows us to identify the relevant variables and describe each regime by a specific simplified model. Models for the tunneling, shuttling and coexistence regime are analyzed separately in the three following subsections. We also give a comparison with the full description in terms of Wigner distributions, current and current-noise to illustrate how the models capture the relevant dynamics.

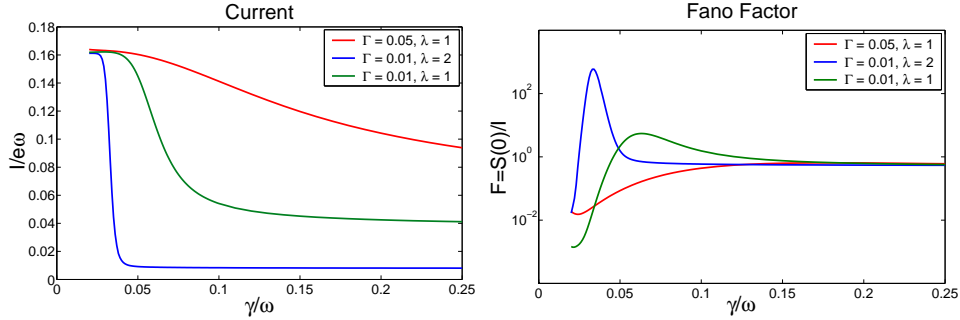


Figure 3. Left panel - Stationary current for the SDQS vs. damping γ . The mechanical dissipation rate γ and the electrical rate $\Gamma = \Gamma_L = \Gamma_R$ are given in units of the mechanical frequency ω , the tunneling length l in terms of $x_0 = \sqrt{\hbar/m\omega}$. The other parameters are $d = 0.5x_0$ and $T = 0$. The current saturates in the shuttling (low damping) regime to one electron per cycle independently from the parameters while is substantially proportional to the bare electrical rate $\Gamma = \Gamma_L = \Gamma_R$ in the tunneling regime (high damping). Right panel - Fano factor for the SDQS vs. damping γ . The curves correspond to the same parameters of the left panel. The very low noise in the shuttling (low damping) regime is a sign of ordered transport. The huge super-poissonian Fano factors correspond to the onset of the coexistence regime. The Figure is taken from [7].

5.1. Renormalized resonant tunneling

The electrical dynamics has the longest time-scale in the tunneling regime since the mechanical relaxation time (which is much longer than the oscillation period) is much shorter than the average injection or ejection time. Because of this time-scale separation, the observation of the device dynamics would most of the time show two mechanically frozen states:

0. Empty dot in the ground state
1. Charged dot moved to the shifted equilibrium position by the constant electrostatic force $e\mathcal{E}$.

We combine this observation with a quantum description of the mechanical oscillator and possible thermal noise under the assumption that the reduced density matrix of the device can be written in the form:

$$\begin{aligned}\sigma_{00}(t) &= p_{00}(t)\sigma_{\text{th}}(0) \\ \sigma_{11}(t) &= p_{11}(t)\sigma_{\text{th}}(e\mathcal{E})\end{aligned}\quad (10)$$

where

$$\sigma_{\text{th}}(\mathcal{F}) = \frac{e^{-\beta(H_{\text{osc}} - \mathcal{F}x)}}{\text{Tr}_{\text{osc}}[e^{-\beta(H_{\text{osc}} - \mathcal{F}x)}]}\quad (11)$$

is the thermal density matrix of a harmonic oscillator subject to an external force \mathcal{F} . The functions $p_{00}(t)$ and $p_{11}(t)$ represent the probability to find the system respectively in the state 0 or 1, respectively. The equations of motion for the probabilities $p_{ii}(t)$ can be derived by inserting the assumption (10) in the definition (7) and taking the

integral over the mechanical degrees of freedom in the corresponding Klein-Kramers equations (9). This results in the rate equations

$$\frac{d}{dt} \begin{pmatrix} p_{00} \\ p_{11} \end{pmatrix} = \begin{pmatrix} \tilde{\Gamma}_R p_{11} - \tilde{\Gamma}_L p_{00} \\ \tilde{\Gamma}_L p_{00} - \tilde{\Gamma}_R p_{11} \end{pmatrix} \equiv \mathcal{L} \begin{pmatrix} p_{00} \\ p_{11} \end{pmatrix} \quad (12)$$

where

$$\begin{aligned} \tilde{\Gamma}_L &= \Gamma_L \text{Tr}_{\text{mech}} \left\{ \sigma_{\text{th}}(0) e^{-\frac{2\hat{x}}{\ell}} \right\} = \Gamma_L \int dq dp e^{-\frac{2q}{\ell}} W_{\text{th}}(q, p) \\ \tilde{\Gamma}_R &= \Gamma_R \text{Tr}_{\text{mech}} \left\{ \sigma_{\text{th}}(e\mathcal{E}) e^{\frac{2\hat{x}}{\ell}} \right\} = \Gamma_R \int dq dp e^{\frac{2q}{\ell}} W_{\text{th}}(q - d, p) \end{aligned} \quad (13)$$

are the renormalized injection and ejection rates and Tr_{mech} indicates the trace over the mechanical degrees of freedom of the device. We have also introduced the Liouvillian operator:

$$\mathcal{L} = \begin{pmatrix} -\tilde{\Gamma}_L & \tilde{\Gamma}_R \\ \tilde{\Gamma}_L & -\tilde{\Gamma}_R \end{pmatrix} \quad (14)$$

The thermal equilibrium Wigner function $W_{\text{th}}(q - d, p)$ is defined as the Wigner representation of the thermal equilibrium density matrix $\sigma_{\text{th}}(e\mathcal{E}) = \sigma_{\text{th}}(m\omega^2 d)$:

$$W_{\text{th}}(q - d, p) = \frac{1}{2\pi m\omega\ell^2} \exp \left\{ -\frac{1}{2} \left[\left(\frac{q-d}{\ell} \right)^2 + \left(\frac{p}{\ell m\omega} \right)^2 \right] \right\} \quad (15)$$

where $\ell = \sqrt{\frac{\hbar}{2m\omega}(2n_B + 1)}$ reduces to the zero point uncertainty length $x_{zp} = \sqrt{\frac{\hbar}{2m\omega}}$ in the zero temperature limit. In the high temperature limit $k_B T \gg \hbar\omega$, ℓ tends to the thermal length $l_{\text{th}} = \sqrt{k_B T / (m\omega^2)}$. Using (15) in (13) gives the renormalized rates:

$$\begin{aligned} \tilde{\Gamma}_L &= \Gamma_L e^{2\left(\frac{\ell}{\ell}\right)^2} \\ \tilde{\Gamma}_R &= \Gamma_R e^{\frac{2d}{\ell} + 2\left(\frac{\ell}{\ell}\right)^2} \end{aligned} \quad (16)$$

Equations (12) describe the dynamics of a resonant tunneling device. All the effects of the movable grain are contained in the effective rates $\tilde{\Gamma}_L, \tilde{\Gamma}_R$. As expected the ejection rate is modified by the ‘‘classical’’ shift d of the equilibrium position due to the electrostatic force on the charged dot. Note that both rates are also *enhanced* by the fuzziness in the position of the oscillator due to thermal and quantum noise. The relevance of this correction is given by the ratio between ℓ and the tunneling length l .

5.1.1. Phase-space distribution The phase space distribution for the stationary state of the simplified model for the tunneling regime is built on the Wigner representation of the thermal density matrix σ_{th} and the stationary solution of the system (12) for the occupation p_{ii} of the electromechanical states i :

$$\begin{aligned} W_{00}^{\text{stat}}(q, p) &= \frac{\tilde{\Gamma}_R}{\tilde{\Gamma}_L + \tilde{\Gamma}_R} W_{\text{th}}(q, p) \\ W_{11}^{\text{stat}}(q, p) &= \frac{\tilde{\Gamma}_L}{\tilde{\Gamma}_L + \tilde{\Gamma}_R} W_{\text{th}}(q - d, p) \end{aligned} \quad (17)$$

The stationary distribution of the tunneling model is determined by the length ℓ and associated momentum $m\omega\ell$, the equilibrium position shift d , the tunneling length l

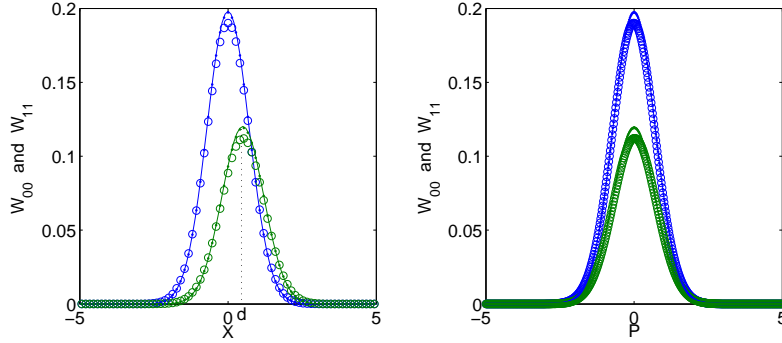


Figure 4. Comparison between the numerical and the analytical results for the Wigner distribution functions. The coordinate (left) or momentum (right) cuts always cross the maximum of the distribution. The green (blue) circles are numerical results in the charged (empty) dot configuration, and the full lines represent the analytical calculations. The parameters are: $\Gamma_L = \Gamma_R = 0.01 \omega$, $\gamma = 0.25 \omega$, $d = 0.5 x_0$, $l = 2 x_0$, $T = 0$. We also plotted with dots the numerical results for $\Gamma = 0.001 \omega$.

and the ratio between left and right bare electrical rates Γ_L/Γ_R . The mechanical relaxation rate γ drops out from the solution and only sets the range of applicability of the simplified model.

In Figures 4 and 5 we compare the Wigner functions calculated both analytically and numerically in the tunneling regime. They show in general a good agreement (Figure 4). The matching is further improved when reducing the bare injection rate $\Gamma_{L,R} = 0.001\omega$ thus enlarging the time scale separation $\Gamma_{L,R} \ll \gamma$ typical of the tunneling regime. The temperature dependence of the stationary Wigner function distribution (Figure 5) verifies the scaling given by the temperature dependent length l .

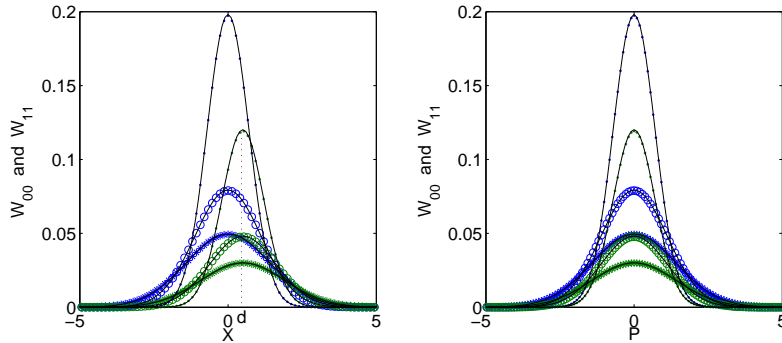


Figure 5. Tunneling Wigner distributions as a function of the temperature. The relevant parameters are: $\gamma = 0.25 \omega$, $\Gamma = 0.001 \omega$, $n_B = 0, 0.75, 1.5$ respectively represented by dots, circles and asterisks. Full lines are the analytical results.

5.1.2. *Current* Since the effect of the oscillator degree of freedom is entirely included in the renormalized rates, the system can be treated formally as a static quantum dot. The time-dependent currents thus read:

$$\begin{aligned} I_R(t) &= \tilde{\Gamma}_R p_{11}(t) \\ I_L(t) &= \tilde{\Gamma}_L p_{00}(t) \end{aligned} \quad (18)$$

In the stationary limit they coincide:

$$I^{\text{stat}} = \tilde{\Gamma}_R p_{11}^{\text{stat}} = \tilde{\Gamma}_L p_{00}^{\text{stat}} = \frac{\tilde{\Gamma}_R \tilde{\Gamma}_L}{\tilde{\Gamma}_L + \tilde{\Gamma}_R} \quad (19)$$

We show in Figure 6 the current calculated numerically and the asymptotic value of the tunneling regime given by Eq. (19).

5.1.3. *Current-noise* We start the calculation with the MacDonald formula for the zero frequency current noise [8, 14, 15]:

$$S(0) = \lim_{t \rightarrow \infty} \frac{d}{dt} \left[\sum_{n=0}^{\infty} n^2 P_n(t) - \left(\sum_{n=0}^{\infty} n P_n(t) \right)^2 \right] \quad (20)$$

where $P_n(t)$ is the probability that n electrons have been collected at time t in the right lead. This probability is connected to the n -resolved probabilities $p_{ii}^{(n)}$ of the two effective states of the tunneling model by the relation:

$$P_n(t) = p_{00}^{(n)}(t) + p_{11}^{(n)}(t) \quad (21)$$

The n -resolved probabilities $p_{ii}^{(n)}$ satisfy the equation of motion:

$$\frac{d}{dt} \begin{pmatrix} p_{00}^{(n)} \\ p_{11}^{(n)} \end{pmatrix} = \begin{pmatrix} \tilde{\Gamma}_R p_{11}^{(n-1)} - \tilde{\Gamma}_L p_{00}^{(n)} \\ \tilde{\Gamma}_L p_{00}^{(n)} - \tilde{\Gamma}_R p_{11}^{(n)} \end{pmatrix} \quad (22)$$

that can be derived by tracing the equation of motion for the total density matrix ρ over bath states with a fixed number (n) of electrons collected in the right lead and finally integrating over the mechanical degrees of freedom. The evaluation of the different terms of the current-noise (20) can be carried out by introducing the generating functions $F_{ii}(t; z) = \sum_n p_{ii}^{(n)}(t) z^n$ [7, 14]. The Fano factor is calculated in terms of the stationary probabilities p_{ii}^{stat} and the pseudoinverse of the Liouvillean (14) $\mathcal{Q}\mathcal{L}^{-1}\mathcal{Q}$.

$$F = 1 - \frac{2}{I^{\text{stat}}} \begin{pmatrix} 1 & 1 \end{pmatrix} \begin{pmatrix} 0 & \tilde{\Gamma}_R \\ 0 & 0 \end{pmatrix} \mathcal{Q}\mathcal{L}^{-1}\mathcal{Q} \begin{pmatrix} 0 & \tilde{\Gamma}_R \\ 0 & 0 \end{pmatrix} \begin{pmatrix} p_{00}^{\text{stat}} \\ p_{11}^{\text{stat}} \end{pmatrix} \quad (23)$$

For a detailed evaluation of the formula (23) we refer the reader to the section IV B of [16]. The resulting Fano factor

$$F = \frac{\tilde{\Gamma}_L^2 + \tilde{\Gamma}_R^2}{(\tilde{\Gamma}_L + \tilde{\Gamma}_R)^2} \quad (24)$$

assumes the familiar form for a tunneling junction, albeit with renormalized rates. In Fig. 6 the value of the Fano factor given by the above formula is depicted as the high-damping asymptote of the full calculation.

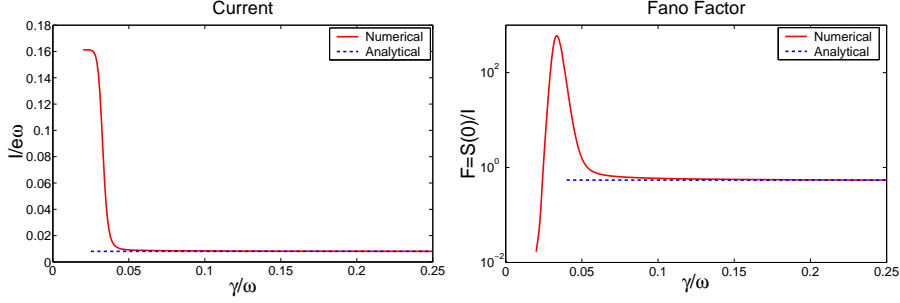


Figure 6. Left panel - Current as a function of the damping for the SDQS. The asymptotic tunneling limit is indicated. The parameters are: $\Gamma_L = \Gamma_R = 0.01\omega$, $\gamma = 0.25\omega$, $d = 0.5x_0$, $l = 2x_0$, $T = 0$. Right panel - Current-noise as a function of the damping for the SDQS. The asymptotic tunneling limit is indicated. The parameters are the same as the ones reported for the current.

5.2. Shuttling: a classical transport regime

The simplified model for the shuttling dynamics is based on the observation – extracted from the full description – that the system exhibits in this operating regime extremely low Fano factors ($F \approx 10^{-2}$): we assume that there is *no noise at all* in the system. Its state is represented by a point that moves on a trajectory in the device phase-space spanned by position, momentum and charge of the oscillating dot. The charge on the oscillating dot is a stochastic variable governed by tunnelling processes, however in the shuttling regime the tunnelling events are effectively deterministic since they are highly probable only at specific times (or positions) defined by the mechanical dynamics.

5.2.1. Equation of motion for the relevant variables We implement the zero noise assumption in the set of coupled Klein-Kramers equations (9) in two steps: we first set $T = 0$ and then simplify the equations further by neglecting all the terms of the \hbar expansion since we assume the classical action of the oscillator to be much larger than the Planck constant. We obtain:

$$\begin{aligned} \frac{\partial W_{00}^{\text{cl}}}{\partial \tau} &= \left[X \frac{\partial}{\partial P} - P \frac{\partial}{\partial X} + \frac{\gamma}{\omega} \frac{\partial}{\partial P} P \right] W_{00}^{\text{cl}} \\ &\quad - \frac{\Gamma_L}{\omega} e^{-2X} W_{00}^{\text{cl}} + \frac{\Gamma_R}{\omega} e^{2X} W_{11}^{\text{cl}} \\ \frac{\partial W_{11}^{\text{cl}}}{\partial \tau} &= \left[\left(X - \frac{d}{l} \right) \frac{\partial}{\partial P} - P \frac{\partial}{\partial X} + \frac{\gamma}{\omega} \frac{\partial}{\partial P} P \right] W_{11}^{\text{cl}} \\ &\quad - \frac{\Gamma_R}{\omega} e^{2X} W_{11}^{\text{cl}} + \frac{\Gamma_L}{\omega} e^{-2X} W_{00}^{\text{cl}} \end{aligned} \quad (25)$$

where we have introduced the dimensionless variables:

$$\tau = \omega t, \quad X = \frac{q}{l}, \quad P = \frac{p}{m\omega l} \quad (26)$$

The superscript “cl” indicates that we are dealing with the classical limit of the Wigner function because of the complete elimination of the quantum “diffusive” terms from

the Klein-Kramers equations. In this spirit, it is natural to try an Ansatz for the Wigner functions, in which the position and momentum dependencies are separable:

$$\begin{aligned} W_{00}^{\text{cl}}(X, P, \tau) &= p_{00}(\tau)\delta(X - X^{\text{cl}}(\tau))\delta(P - P^{\text{cl}}(\tau)) \\ W_{11}^{\text{cl}}(X, P, \tau) &= p_{11}(\tau)\delta(X - X^{\text{cl}}(\tau))\delta(P - P^{\text{cl}}(\tau)) \end{aligned} \quad (27)$$

where the trace over the system phase-space sets the constraint $p_{00} + p_{11} = 1$. The variables X^{cl} and P^{cl} represent the position and momentum of the (center of mass) of the oscillating dot; $p_{11(00)}$ is the probability for the quantum dot to be charged (empty).

By inserting the Ansatz (27) into equation (25) and matching the coefficients of the terms proportional to $\delta \times \delta$ we obtain the equations of motion for the charge probabilities p_{ii} :

$$\begin{aligned} \dot{p}_{00} &= -\frac{\Gamma_L}{\omega}e^{-2X^{\text{cl}}}p_{00} + \frac{\Gamma_R}{\omega}e^{2X^{\text{cl}}}p_{11} \\ \dot{p}_{11} &= \frac{\Gamma_L}{\omega}e^{-2X^{\text{cl}}}p_{00} - \frac{\Gamma_R}{\omega}e^{2X^{\text{cl}}}p_{11} \end{aligned} \quad (28)$$

Matching the coefficients proportional to the distributions $\delta \times \delta'$ (here δ' is the derivative of the delta-function) yields the equations for the mechanical degrees of freedom:

$$\begin{aligned} p_{00}\dot{X}^{\text{cl}} &= p_{00}P^{\text{cl}} \\ p_{11}\dot{X}^{\text{cl}} &= p_{11}P^{\text{cl}} \\ p_{00}\dot{P}^{\text{cl}} &= p_{00}\left(-X^{\text{cl}} - \frac{\gamma}{\omega}P^{\text{cl}}\right) \\ p_{11}\dot{P}^{\text{cl}} &= p_{11}\left(-X^{\text{cl}} + \frac{d}{\lambda} - \frac{\gamma}{\omega}P^{\text{cl}}\right) \end{aligned} \quad (29)$$

The equations involving \dot{P}^{cl} have a solution only if

$$p_{00}p_{11} = 0 \quad (30)$$

combined with the normalization condition $p_{00} + p_{11} = 1$. Under these conditions the system (29) is equivalent to

$$\begin{aligned} \dot{X}^{\text{cl}} &= P^{\text{cl}} \\ \dot{P}^{\text{cl}} &= -X^{\text{cl}} + \frac{d}{\lambda}p_{11} - \frac{\gamma}{\omega}P^{\text{cl}} \end{aligned} \quad (31)$$

The condition (30) also follows by substituting the Ansatz (27) into the equations (25) and by using the equations of motion (31) and (28). This shows that (30) also sets the limits of the validity of the Ansatz (27). However, the only differentiable solution for (30) is $p_{00} = 0$ or $p_{11} = 0$ for all times, which is not compatible with the equation of motion (28). Thus, the Ansatz (27) does not yield exact solutions to the original equations (25).

While an exact solution has not been found, we can still proceed with the following physical argument. Suppose now that the switching time between the two allowed states, $p_{11} = 1; p_{00} = 0$ or $p_{00} = 1; p_{11} = 0$, is much shorter than the shortest mechanical time (the oscillator period $T = 2\pi/\omega$). A solution of the system of equations (31) and (28) with this time scale separation would satisfy the condition (30) ‘‘almost everywhere’’ and, when inserted into (27) would represent a solution for (25).

We rewrite the set of equations (31) and (28) as:

$$\begin{aligned}\dot{X} &= P \\ \dot{P} &= -X + d^*Q - \gamma^*P \\ \dot{Q} &= \Gamma_L^*e^{-2X}(1-Q) - \Gamma_R^*e^{2X}Q\end{aligned}\quad (32)$$

where we have dropped the ‘‘cl’’ superscript, renamed $p_{11} \equiv Q$, used the trace condition $p_{00} = 1 - p_{11}$, and defined the rescaled parameters: $d^* = d/l$, $\gamma^* = \gamma/\omega$, $\Gamma_{L,R}^* = \Gamma_{L,R}/\omega$. In the following section we analyze the dynamics implied by Eq. (32).

5.2.2. Stable limit cycles Here we give the results of a numerical solution of Eq. (32) for different values of the parameters and different initial conditions. For the parameter values that correspond to the fully developed shuttling regime, the system has a limit cycle solution with the desirable time scale separation we discussed in the previous section. Figure 7 shows the typical appearance of the limit cycle.

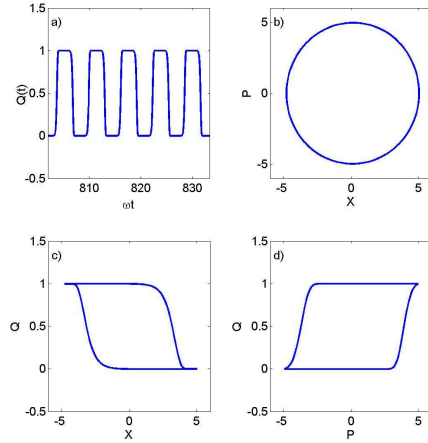


Figure 7. Different representations of the limit cycle solution of the system of differential equations (32) that describes the shuttling regime. For a detailed description see the text. X is the coordinate in units of the tunneling length l , while P is the momentum in units of $m\omega l$.

In Fig. 7(a) we show the charge $Q(\tau)$ as a function of time. The charge value is jumping periodically from 0 to 1 and back with a period equal to the mechanical period. The transition itself is almost instantaneous. In panels (b), (c) and (d) three different projections of the 3D-phase-space trajectory are reported and the time evolution along them is intended clockwise. The X, P projection shows the characteristic circular trajectory of harmonic oscillations. In the X, Q (P, Q) projection the position(momentum)-charge correlation is visible.

The full description of the SDQS in the shuttling regime has a phase space visualization in terms of a ring shaped *stationary* total Wigner distribution function, see Fig. 2. We can interpret this fuzzy ring as the probability distribution obtained

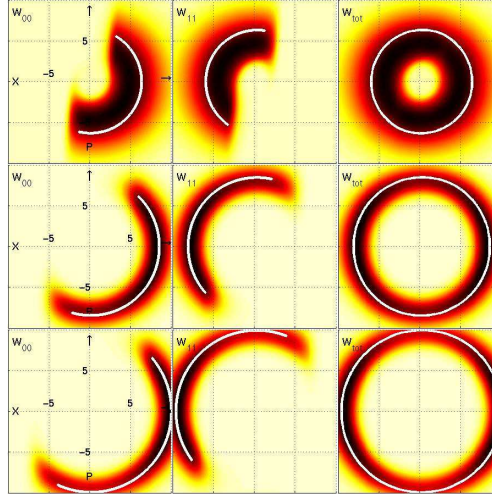


Figure 8. Correspondence between the Wigner function representation and the simplified trajectory limit for the shuttling regime. The white ring is the (X, P) projection of the limit cycle. The $Q = 1$ and $Q = 0$ portions of the trajectory are visible in the charged and empty dot graphs respectively. The parameters are $\gamma = 0.02\omega$, $d = 0.5x_0$, $\Gamma = 0.05\omega$, $l = x_0$ in the upper row, $\gamma = 0.02\omega$, $d = 0.5x_0$, $\Gamma = 0.05\omega$, $l = 2x_0$ in the central row and $\gamma = 0.02\omega$, $d = 0.5x_0$, $\Gamma = 0.01\omega$, $l = 2x_0$ in the lower row.

from many different noisy realizations of (quasi) limit cycles. The stationary solution for the Wigner distribution is the result of a diffusive dynamics on an effective “Mexican hat” potential that involves both amplitude and phase of the oscillations. In the noise-free semiclassical approximation we turn off the diffusive processes and the point-like state describes in the shuttling regime a single trajectory with a definite constant amplitude and *periodic* phase. We expect this trajectory to be the average of the noisy trajectories represented by the Wigner distribution. In the third column of Fig. 8 the total Wigner function corresponding to different parameter realization of the shuttling regime is presented. The white circle is the semiclassical trajectory. In the first two columns the asymmetric sharing of the ring between the charged and empty states is also compared with the corresponding $Q = 1$ and $Q = 0$ portions of the semiclassical trajectory.

In the semiclassical description we also have direct access to the current as a function of the time. For example the right lead current reads:

$$I_R(\tau) = Q(\tau)\Gamma_R e^{2X(\tau)} \quad (33)$$

and is also a periodic function with peaks in correspondence to the unloading processes. The integral of $I_R(\tau)$ over one mechanical period is 1 and represents the number of electron shuttled per cycle by the oscillating dot, in complete agreement with the full description.

5.3. Coexistence: a dichotomous process

The longest time-scale in the coexistence regime corresponds to infrequent switching between the shuttling and the tunneling regime, see Fig. 9. The amplitude of the dot oscillations is the relevant variable that is recording this slow dynamics. We analyze this particular operating regime of the SDQS in four steps. (i) We first explore the consequences of the slow switching in terms of current and current noise. (ii) Next, we derive the effective bistable potential which controls the dynamics of the oscillation amplitude. (iii) We then apply Kramers' theory for escape rates to this effective potential and calculate the switching rates between the two amplitude metastable states corresponding to the local minima of the potential. (iv) We conclude the section by comparing the (semi)analytical results of the simplified model with the numerical calculations for the full model.

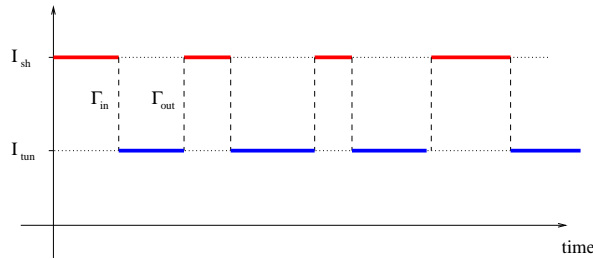


Figure 9. Schematic representation of the time evolution of the current in the dichotomous process between current modes in the SDQS coexistence regime. The relevant currents are the shuttling (I_{sh}) and the tunneling (I_{tun}) currents, respectively. The switching rates Γ_{in} and Γ_{out} correspond to switching in and out of the tunneling mode.

5.3.1. Two current modes Let us consider a bistable system with two different modes that we call for convenience *Shuttling* (sh) and *Tunneling* (tun) and two different currents I_{sh} and I_{tun} , respectively, associated with these modes. The system can switch between the shuttling and the tunneling mode randomly, but with definite rates: namely Γ_{in} for the process “shuttling \rightarrow tunneling” and Γ_{out} for the opposite, “tunneling \rightarrow shuttling”. We collect this information in the master equation:

$$\dot{\mathbf{P}} = \frac{d}{dt} \begin{pmatrix} P_{\text{sh}} \\ P_{\text{tun}} \end{pmatrix} = \begin{pmatrix} -\Gamma_{\text{in}} & \Gamma_{\text{out}} \\ \Gamma_{\text{in}} & -\Gamma_{\text{out}} \end{pmatrix} \begin{pmatrix} P_{\text{sh}} \\ P_{\text{tun}} \end{pmatrix} = \mathbf{LP} \quad (34)$$

For such a system the average current and the Fano factor read [14, 17]:

$$\begin{aligned} I^{\text{stat}} &= \frac{I_{\text{sh}}\Gamma_{\text{out}} + I_{\text{tun}}\Gamma_{\text{in}}}{\Gamma_{\text{in}} + \Gamma_{\text{out}}} \\ F &= \frac{S(0)}{I^{\text{stat}}} = 2 \frac{(I_{\text{sh}} - I_{\text{tun}})^2}{I_{\text{sh}}\Gamma_{\text{out}} + I_{\text{tun}}\Gamma_{\text{in}}} \frac{\Gamma_{\text{in}}\Gamma_{\text{out}}}{(\Gamma_{\text{in}} + \Gamma_{\text{out}})^2} \end{aligned} \quad (35)$$

The framework of the simplified model for the coexistence regime is given by these formulas. The task is now to identify the two modes in the dynamics of the shuttle device and, above all, calculate the switching rates. This can be done by using the Kramers' escape rates for a bistable effective potential.

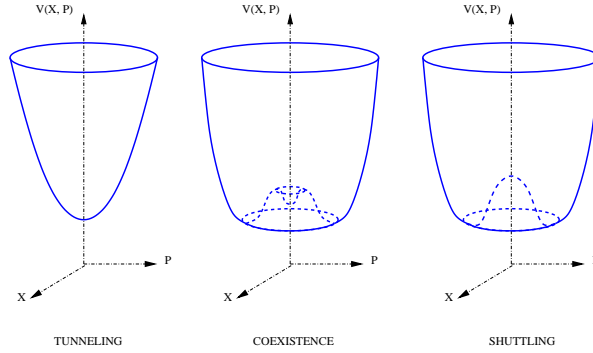


Figure 10. Schematic representation of the effective potentials for the three operating regimes.

5.3.2. Effective potential The tunneling to shuttling crossover visualized by the total Wigner function distribution (Fig. 2) can be understood in terms of an effective stationary potential in the phase space generated by the non-linear dynamics of the shuttle device. We show in Fig. 10 the three qualitatively different shapes of the potential surmised from the observation of the stationary Wigner functions associated with the three operating regimes. Recently Fedorets *et al.* [5] initiated the study of the tunneling-shuttling transition in terms of an effective radial potential. Taking inspiration from their work we extend the analysis to the slowest *dynamics* in the device and use quantitatively the idea of the effective potential for the description of the coexistence regime.

In the process of elimination of the fast variables we start from the Klein-Kramers equations for the SDQS that we rewrite symmetrized by shifting the coordinates origin to $d/2$:

$$\begin{aligned}
\frac{\partial W_{00}}{\partial t} &= \left[m\omega^2 \left(q + \frac{d}{2} \right) \frac{\partial}{\partial p} - \frac{p}{m} \frac{\partial}{\partial q} + \gamma \frac{\partial}{\partial p} p + \gamma m \hbar \omega \left(n_B + \frac{1}{2} \right) \frac{\partial^2}{\partial p^2} \right] W_{00} \\
&\quad + \Gamma_R e^{2q/l} W_{11} - \Gamma_L e^{-2q/l} \sum_{n=0}^{\infty} \frac{(-1)^n}{(2n)!} \left(\frac{\hbar}{l} \right)^{2n} \frac{\partial^{2n} W_{00}}{\partial p^{2n}} \\
\frac{\partial W_{11}}{\partial t} &= \left[m\omega^2 \left(q - \frac{d}{2} \right) \frac{\partial}{\partial p} - \frac{p}{m} \frac{\partial}{\partial q} + \gamma \frac{\partial}{\partial p} p + \gamma m \hbar \omega \left(n_B + \frac{1}{2} \right) \frac{\partial^2}{\partial p^2} \right] W_{11} \\
&\quad + \Gamma_L e^{-2q/l} W_{00} - \Gamma_R e^{2q/l} \sum_{n=0}^{\infty} \frac{(-1)^n}{(2n)!} \left(\frac{\hbar}{l} \right)^{2n} \frac{\partial^{2n} W_{11}}{\partial p^{2n}}
\end{aligned} \tag{36}$$

where the renormalization of the tunneling rates due to the coordinate shift has been absorbed in a redefinition of the Γ 's. The idea is to get rid of the variables that due to their fast dynamics are not relevant for the description of the coexistence regime. In equations (36) we describe the electrical state of the dot as empty or charged. We switch to a new set of variables with the definition:

$$W_{\pm} = W_{00} \pm W_{11} \tag{37}$$

In absence of the harmonic oscillator the state $|+\rangle$ would be fixed by the trace sum rule and the state $|-\rangle$ would relax to zero on a time scale fixed by the tunneling rates. We

assume that also in the presence of the mechanical degree of freedom the relaxation dynamics of the $|-\rangle$ state is much faster than the one of the $|+\rangle$ state.

In the dimensionless phase space given by the coordinates X and P of (26) we switch to the polar coordinates defined by the relations [5]:

$$X = A \sin \phi \quad P = A \cos \phi \quad (38)$$

Since we are interested only in the dynamics of the amplitude in the phase space (the slowest in the coexistence regime) we introduce the projector \mathcal{P}_ϕ that averages over the phase :

$$\mathcal{P}_\phi[\bullet] = \frac{1}{2\pi} \int_0^{2\pi} d\phi \bullet \quad (39)$$

We also need the orthogonal complement $\mathcal{Q}_\phi = 1 - \mathcal{P}_\phi$. Using these two operators we decompose the Wigner distribution function into:

$$W_+ = \mathcal{P}_\phi W_+ + \mathcal{Q}_\phi W_+ = \bar{W}_+ + \tilde{W}_+ \quad (40)$$

Finally we make a perturbation expansion of (36) in the small parameters:

$$\frac{d}{l} \ll 1, \quad \left(\frac{x_0}{l}\right)^2 \ll 1, \quad \frac{\gamma}{\omega} \ll 1 \quad (41)$$

These three inequalities correspond to the three physical assumptions:

- (i) The external electrostatic force is a small perturbation of the harmonic oscillator restoring force in terms of the sensitivity to displacement of the tunneling rates. This justifies an oscillator-independent treatment of the tunneling regime.
- (ii) The tunneling length is large compared to the zero point fluctuations. Since the oscillator dynamics for the shuttling regime (and then partially also for the coexistence regime) happens on the scale of the tunneling length, this condition ensures a quasi-classical behaviour of the harmonic oscillator.
- (iii) The coupling of the oscillator to the thermal bath is weak and the oscillator dynamics is under-damped.

Using these approximations the Klein-Kramers equations (36) reduce (for details see, *e.g.*, [5, 14]) to the form:

$$\partial_\tau \bar{W}_+(A, \tau) = \frac{1}{A} \partial_A A [V'(A) + D(A) \partial_A] \bar{W}_+(A, \tau) \quad (42)$$

where $V'(A) = \frac{d}{dA} V(A)$ and $D(A)$ are given functions of A . Before calculating explicitly the functions V' and D we explore the consequences of the formulation of the Klein-Kramers equations (36) in the form (42). The stationary solution of the equation (42) reads [5]:

$$\bar{W}_+^{\text{stat}}(A) = \frac{1}{\mathcal{Z}} \exp \left(- \int_0^A dA' \frac{V'(A')}{D(A')} \right) \quad (43)$$

where \mathcal{Z} is the normalization that ensures the integral of the phase-space distribution to be unity: $\int_0^\infty dA' 2\pi A' \bar{W}_+^{\text{stat}}(A') = 1$. Equation (42) is identical to the Fokker-Planck equation for a particle in the two-dimensional rotationally invariant potential V (see Fig. 10) with stochastic forces described by the (position dependent) diffusion

coefficient D . All contributions to the effective potential V and diffusion coefficient D can be grouped according to the power of the small parameters that they contain.

$$\begin{aligned} V'(A) &= \frac{\gamma}{\omega} \frac{A}{2} + \frac{d}{2l} \alpha_0(A) + \left(\frac{x_0}{l}\right)^4 \alpha_1(A) + \left(\frac{d}{2l}\right)^2 \alpha_2(A) + \frac{\gamma}{\omega} \frac{d}{2l} \alpha_3(A) \\ D(A) &= \frac{\gamma}{\omega} \left(\frac{x_0}{l}\right)^2 \frac{1}{2} \left(n_B + \frac{1}{2}\right) + \left(\frac{x_0}{l}\right)^4 \beta_1(A) + \left(\frac{d}{2l}\right)^2 \beta_2(A) + \frac{\gamma}{\omega} \frac{d}{2l} \beta_3(A) \end{aligned} \quad (44)$$

where the α functions read:

$$\begin{aligned} \alpha_0 &= \mathcal{P}_\phi \cos \phi \hat{G}_0 \Gamma_- \\ \alpha_1 &= -\frac{1}{4} \mathcal{P}_\phi \cos \phi \Gamma_- \partial_P (\hat{G}_0 \Gamma_-) \\ \alpha_2 &= \mathcal{P}_\phi \cos \phi \hat{G}_0 \Gamma_- \hat{g}_0 \mathcal{Q}_\phi \partial_P (\hat{G}_0 \Gamma_-) \\ \alpha_3 &= \mathcal{P}_\phi \cos \phi \left[\hat{G}_0^2 \Gamma_- + A \hat{G}_0 \partial_P (\hat{G}_0 \Gamma_-) - \frac{A}{2} \sin \phi \partial_P (\hat{G}_0 \Gamma_-) \right] \end{aligned} \quad (45)$$

and the β 's can be written as:

$$\begin{aligned} \beta_1 &= \frac{1}{4} \mathcal{P}_\phi \cos^2 \phi \left[\Gamma_+ - \Gamma_- \hat{G}_0 \Gamma_- \right] \\ \beta_2 &= \mathcal{P}_\phi \cos \phi \left[\hat{G}_0 \cos \phi + \hat{G}_0 \Gamma_- \hat{g}_0 \mathcal{Q}_\phi \cos \phi \hat{G}_0 \Gamma_- \right] \\ \beta_3 &= A \mathcal{P}_\phi \cos \phi \left[\hat{G}_0 \cos^2 \phi \hat{G}_0 \Gamma_- + \frac{1}{4} \hat{G}_0 \Gamma_- \sin 2\phi - \frac{1}{4} \sin 2\phi \hat{G}_0 \Gamma_- \right] \end{aligned} \quad (46)$$

where

$$\begin{aligned} \Gamma_\pm &= \Gamma_L e^{-2A \sin \phi} \pm \Gamma_R e^{2A \sin \phi} \\ \hat{g}_0 &= (\partial_\phi)^{-1} \\ \hat{G}_0 &= (\partial_\phi + \Gamma_+)^{-1} \end{aligned} \quad (47)$$

The α and β functions are calculated by isolating in the Liouvillean for the distribution \bar{W}_+ the driving and diffusive components with generic forms

$$\frac{1}{A} \partial_A A \{ \alpha_i(A) \} \quad (48)$$

and

$$\frac{1}{A} \partial_A A \{ \beta_i(A) \} \partial_A \quad (49)$$

respectively. As an example we give the derivation of the functions α_3 and β_3 . We start by rewriting the equation of motion (42) for the distribution \bar{W}_+ in the form:

$$\partial_\tau \bar{W}_+ = \mathcal{L}[\bar{W}_+] \approx (\mathcal{L}^I + \mathcal{L}^{II})[\bar{W}_+] \quad (50)$$

where we have distinguished the Liouvilleans of first and second order in the small parameter expansion (41). The contribution $\frac{2}{\omega} \frac{d}{l}$ of the second order Liouvillean \mathcal{L}^{II} reads:

$$\mathcal{L}_{\gamma d} = \mathcal{P}_\phi \partial_P [\hat{G}_0 \partial_P P \hat{G}_0 \Gamma_- + P \hat{g}_0 \mathcal{Q}_\phi \partial_P \hat{G}_0 \Gamma_- + \hat{G}_0 \Gamma_- \hat{g}_0 \mathcal{Q}_\phi \partial_P P] \quad (51)$$

and represents the starting point for the calculation of the functions α_3 and β_3 . We express then the differential operators ∂_P in polar coordinates and take into account that the Liouvillean is applied to a function \bar{W}_+ independent of the variable ϕ :

$$\begin{aligned} \mathcal{L}_{\gamma d} = & \frac{1}{A} \partial_A A \mathcal{P}_\phi \cos \phi \left[\hat{G}_0^2 \Gamma_- + \hat{G}_0 A \cos \phi \partial_P (\hat{G}_0 \Gamma_-) + \hat{G}_0 A \cos^2 \phi \hat{G}_0 \Gamma_- \partial_A \right. \\ & + A \cos \phi \hat{g}_0 \mathcal{Q}_\phi \partial_P (\hat{G}_0 \Gamma_-) + A \cos \phi \hat{g}_0 \mathcal{Q}_\phi \cos \phi \hat{G}_0 \Gamma_- \partial_A \\ & \left. + \hat{G}_0 \Gamma_- \hat{g}_0 \mathcal{Q}_\phi A \cos^2 \phi \partial_A \right] \end{aligned} \quad (52)$$

Finally, we separate in (52) the driving term from the diffusive contributions and thus identify the functions α_3 and β_3 ‡:

$$\begin{aligned} \mathcal{L}_{\gamma d} = & \frac{1}{A} \partial_A A \left\{ \mathcal{P}_\phi \cos \phi \left[\hat{G}_0^2 \Gamma_- + A \hat{G}_0 \partial_P (\hat{G}_0 \Gamma_-) - \frac{A}{2} \sin \phi \partial_P (\hat{G}_0 \Gamma_-) \right] \right\} + \\ & \frac{1}{A} \partial_A A \left\{ \mathcal{P}_\phi \cos \phi \left[\hat{G}_0 \cos^2 \phi \hat{G}_0 \Gamma_- + \frac{1}{4} \hat{G}_0 \Gamma_- \sin 2\phi - \frac{1}{4} \sin 2\phi \hat{G}_0 \Gamma_- \right] \right\} \partial_A \end{aligned} \quad (53)$$

Some of these results appear also in the work by Fedorets *et al.* [5]. Since we have projected out the phase ϕ we are effectively working in a one-dimensional phase space given by the amplitude A . Note however that Eq. (42) though is *not* as it stands a Kramers equation for a single variable. This is related to the fact that also the distribution \bar{W}_+ is *not* the amplitude distribution function, but, so to speak, a cut at fixed phase of a two dimensional rotationally invariant distribution. The difference is a geometrical factor A . We define the amplitude probability distribution $\mathcal{W}(A, \tau) = A \bar{W}_+(A, \tau)$ and insert this definition in equation (42). We obtain:

$$\begin{aligned} \partial_\tau \mathcal{W}(A, \tau) &= \partial_A A [V'(A) + D(A) \partial_A] \frac{1}{A} \mathcal{W}(A, \tau) \\ &= \partial_A [\mathcal{V}'(A) + D(A) \partial_A] \mathcal{W}(A, \tau) \end{aligned} \quad (54)$$

where we have defined the geometrically corrected potential

$$\mathcal{V}(A) = V(A) - \int_{A_0}^A \frac{D(A')}{A'} dA' \quad (55)$$

which for an amplitude independent diffusion coefficient gives a corrected potential diverging logarithmically in the origin. The lower limit of integration is arbitrary and reflects the arbitrary constant in the definition of the potential. The equation (54) is the one-dimensional Kramers equation that constitutes the starting point for the calculation of the switching rates that characterize the coexistence regime.

The effective potential \mathcal{V} that we obtained has, for parameters that correspond to the coexistence regime, a typical double-well shape (see *e.g.* the left panel of figure 11). We assume for a while the diffusion constant to be independent of the amplitude A . In this approximation the stationary solution of the equation (54) reads:

$$\mathcal{W}^{\text{stat}}(A) = \frac{1}{\mathcal{Z}} \exp \left(-\frac{\mathcal{V}(A)}{D} \right) \quad (56)$$

where \mathcal{Z} is the normalization: $\mathcal{Z} = \int_0^\infty \exp \left(-\frac{\mathcal{V}(A)}{D} \right) dA$. The probability distribution is concentrated around the minima of the potential and has a minimum at the potential

‡ In this step of the derivation we have also used the projector \mathcal{P}_ϕ to define a scalar product $\mathcal{P}_\phi f(\phi)g(\phi) \equiv (f, g)$ and the adjoint relation: $(f, \hat{O}g) = (\hat{O}^\dagger f, g)$.

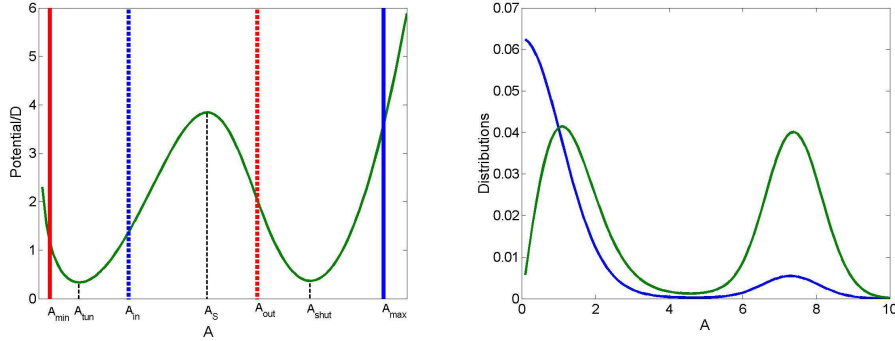


Figure 11. *Left panel – Bistable effective potential for the SDQS coexistence regime. The important amplitudes for the calculation of the rates are indicated. In red (blue) are indicated the reflecting (full) and absorbing (dashed) borders for the calculation of the $\Gamma_{\text{out,(in)}}$ escape rate. Right panel – Example of the stationary distribution W_+^{stat} (blue) and the amplitude distribution W^{stat} (green) for the SDQS in the coexistence regime. The tunneling and shuttling states are in both cases well separated.*

barrier (see *e.g.* the right panel of Fig. 11). If this potential barrier is high enough (*i.e.* $V_{\text{max}} - V_{\text{min}} \gg D$) we clearly identify two distinct states with definite average amplitude: the lower amplitude state corresponding to the tunneling regime and the higher to the shuttling.

The coexistence regime of a SDQS is mapped into a classical model for a particle moving in a bistable potential \mathcal{V} with random forces described by the diffusion constant D . The correspondent escape rates from the tunneling to the shuttling mode (Γ_{out}) and back (Γ_{in}) can be calculated using the standard theory of Mean First Passage Time (MFPT) for a random variable [18]:

$$\begin{aligned} \Gamma_{\text{out}} &= D \left(\int_{A_{\text{tun}}}^{A_{\text{out}}} dB e^{\frac{\mathcal{V}(B)}{D}} \int_{A_{\text{min}}}^B dA e^{-\frac{\mathcal{V}(A)}{D}} \right)^{-1} \\ \Gamma_{\text{in}} &= D \left(\int_{A_{\text{in}}}^{A_{\text{shut}}} dB e^{\frac{\mathcal{V}(B)}{D}} \int_B^{A_{\text{max}}} dA e^{-\frac{\mathcal{V}(A)}{D}} \right)^{-1} \end{aligned} \quad (57)$$

where integration limits of equation (57) are graphically represented in the left panel of Fig. 11. We can now insert the explicit expression for the switching rates Γ_{in} and Γ_{out} in Eq. (35) and obtain in this way the current and Fano factor for the coexistence regime. They represent, together with the stationary distribution (56) the main result of this section and allow us for a quantitative comparison between the simplified model and the full description of the coexistence regime.

5.3.3. Comparison The phase space distribution is the most sensitive object to compare the model and the full description. One of the basic procedures adopted in the derivation of the Kramers equation (54) is the expansion to second order in the small parameters (41). In order to test the reliability of the model we simplify as much as possible the description reducing the model to a classical description:

namely taking the zero limit for the parameter $(\frac{x_0}{l})$. We realize physically this condition assuming a large temperature and a tunneling length l of the order of the thermal length $l_{\text{th}} = \sqrt{\frac{k_B T}{m\omega^2}}$. Also the full description is slightly changed, but not qualitatively: the three regimes are still clearly present with their characteristics. The numerical calculation of the stationary density matrix is though based on a totally different approach. In the quantum regime we used the Arnoldi iteration scheme for the numerically demanding calculation of the null vector of the big ($10^4 \times 10^4$) matrix representing the Liouvillean [4, 7]. Problems concerning the convergence of the Arnoldi iteration due to the delicate issue of preconditioning forced us to abandon this method in the classical case. We adopted instead the continued fraction method [18]. In Figs. 12, 13 and 14 we present the results for the stationary Wigner function,

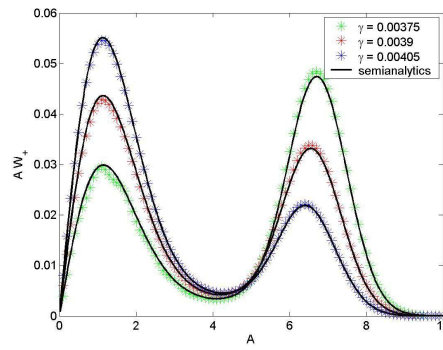


Figure 12. Stationary amplitude probability distribution \mathcal{W} for the SDQS in the coexistence regime. We compare the results obtained from the simplified model (full line) and from the full description (asterisks). These results are obtained in the classical high temperature regime $k_B T \gg \hbar\omega$. The amplitude is measured in units of $l_{\text{th}} = \sqrt{\frac{k_B T}{m\omega^2}}$. The mechanical damping γ in units of the mechanical frequency ω . The other parameter values are $d = 0.05 l_{\text{th}}$ and $\Gamma = 0.015 \omega$, $\lambda = 2 \lambda_{\text{th}}$.

the current and the Fano factor, respectively, in the semiclassical approximation and in the full description.

Deep in the quantum regime the coexistence regime (*e.g.* Fig. 2 where the amplitude of the shuttling oscillations is $\approx 7x_0$) is not captured quantitatively with the simplified model. Given that the concept of elimination of the fast dynamics is still valid, we believe that the discrepancy indicates that the expansion in the small parameters has not been carried out to sufficiently high order. The effective potential calculated from a second order expansion still gives the position of the ring structure with reasonable accuracy but the overall stationary Wigner function is not fully reproduced due to an inaccurate diffusion function $D(A)$. One should thus consider higher order terms in the parameter $(x_0/l)^2$. A higher order expansion, however, represents a fundamental problem since it would produce terms with higher order derivatives with respect to the amplitude A in the Fokker-Planck equation and, consequently, a straight forward application of the escape time theory is no longer possible.

It has nevertheless been demonstrated [9] with the help of the higher cumulants

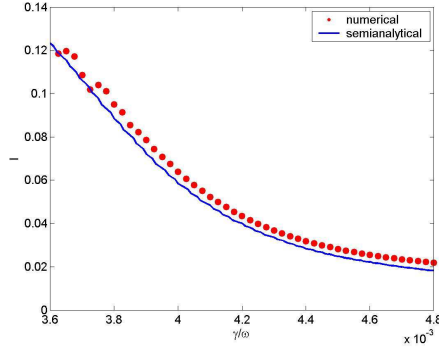


Figure 13. Current in the coexistence regime of SDQS. Comparison between semianalytical and full numerical description. For the parameter values see Fig. 12.

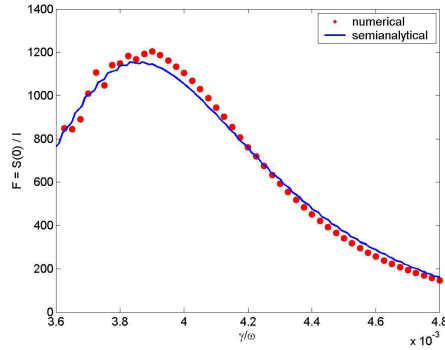


Figure 14. Fano factor in the coexistence regime of SDQS. Comparison between semianalytical and full numerical description. For the parameter values see Fig. 12.

of the current that the description of the coexistence regime as a dichotomous process is valid also deep in the quantum regime ($l = 1.5x_0$), the only necessary condition being a separation of the ring and dot structures in the stationary Wigner function distribution.

We observe that the second order expansion for the effective potential (41) is essentially converged, and able to give the correct position of the shuttling ring also in the quantum regime. From Eq. (43) it is clear that a strongly amplitude dependent diffusion constant $D(A)$ would destroy this agreement. We conjecture that a higher order expansion may lead to an effective renormalization of the diffusion constant. To test this idea we used the diffusion constant as a fitting parameter, and found that the current and the Fano factor are very accurately reproduced by using a fitted diffusion constant, with a value approximately twice larger than the one calculated at zero temperature and in second order in the small parameters. Clearly, further work is needed to find out whether the agreement is due to fortuitous coincidence, or if a

physical justification can be given to this conjecture. Also, an investigation of whether the results obtained in the classical limit are extendable to the quantum limit by a controlled renormalization of the diffusion constant is called for.

6. Conclusions

The specific separation of time scales in the different regimes allowed us to identify the relevant variables and describe each regime by a specific *simplified model*. In the tunneling (high damping) regime the mechanical degree of freedom is almost frozen and all the features revealed by the Wigner distribution, the current and the current noise can be reproduced with a resonant tunneling model with tunneling rates renormalized due to the movable quantum dot. Most of the features of the shuttling regime (self-sustained oscillations, charge-position correlation) are captured by a simple model derived as the zero-noise limit of the full description. Finally for the coexistence regime we proposed a dynamical picture in terms of slow dichotomous switching between the tunneling and shuttling modes. This interpretation was mostly suggested by the presence in the stationary Wigner function distributions of both the characteristic features of the tunneling and shuttling dynamics and by a corresponding gigantic peak in the Fano factor. We based the derivation of the simplified model on the fast variables elimination from the Klein-Kramers equations for the Wigner function and a subsequent derivation of an effective bistable potential for the amplitude of the dot oscillation (the relevant slow variable in this regime).

The comparison of the results obtained using the simplified models with the full description in terms of Wigner distributions, current and current-noise proves that the models, at least in the limits set by the chosen investigation tools, capture the relevant features of the shuttle dynamics.

The work of T. N. is a part of the research plan MSM 0021620834 that is financed by the Ministry of Education of the Czech Republic, and A. D. acknowledges financial support from the Deutsche Forschungsgemeinschaft within the framework of the Graduiertenkolleg “Nichtlinearität und Nichtgleichgewicht in kondensierter Materie” (GRK 638).

References

- [1] L. Y. Gorelik, A. Isacsson, M. V. Voinova, B. Kasemo, R. I. Shekhter, and M. Jonson, Shuttle Mechanism for Charge Transfer in Coulomb Blockade Nanostructures, *Phys. Rev. Lett.* **80**(20), 4526 (May 1998).
- [2] D. V. Scheible, A. Erbe, and R. H. Blick, Tunable coupled nanomechanical resonators for single-electron transport, *New Journal of Physics* **4**, 86 (2002).
- [3] A. D. Armour and A. MacKinnon, Transport via a quantum shuttle, *Phys. Rev. B* **66**(3), 035333 (July 2002).
- [4] T. Novotný, A. Donarini, and A.-P. Jauho, Quantum Shuttle in Phase Space, *Phys. Rev. Lett.* **90**(25), 256801 (June 2003).
- [5] D. Fedorets, L. Y. Gorelik, R. I. Shekhter, and M. Jonson, Quantum Shuttle Phenomena in a Nanoelectromechanical Single-Electron Transistor, *Phys. Rev. Lett.* **92**(16), 166801 (April 2004).
- [6] F. Pistolesi, Full counting statistics of a charge shuttle, *Phys. Rev. B* **69**(24), 245409 (June 2004).
- [7] T. Novotný, A. Donarini, C. Flindt, and A.-P. Jauho, Shot Noise of a Quantum Shuttle, *Phys. Rev. Lett.* **92**(24), 248302 (June 2004).
- [8] C. Flindt, T. Novotný, and A.-P. Jauho, Current noise in a vibrating quantum dot array, *Phys. Rev. B* **70**, 205334 (November 2004).

- [9] C. Flindt, T. Novotný, and A.-P. Jauho, Full counting statistics of nano-electromechanical systems, *Europhys. Lett.* **69**(3), 475 (December 2004).
- [10] F. Pistolesi and R. Fazio, Charge shuttle as a nanomechanical rectifier, *Phys. Rev. Lett.* **94**, 036806 (January 2005).
- [11] D. Fedorets, L. Y. Gorelik, R. I. Shekhter, and M. Jonson, Spintronics of a Nanoelectromechanical Shuttle, *Phys. Rev. Lett.* **95**(5), 057203 (July 2005).
- [12] A. Erbe, C. Weiss, W. Zwerger, and R. H. Blick, Nanomechanical Resonator Shuttling Single Electrons at Radio Frequencies, *Phys. Rev. Lett.* **87**(9), 096106 (August 2001).
- [13] D. V. Scheible and R. Blick, Silicon nanopillars for mechanical single-electron transport, *Appl. Phys. Lett.* **84**(23), 4632 (June 2004).
- [14] A. Donarini, *Dynamics of Shuttle Devices*, PhD thesis, MIC, Technical University of Denmark, October 2004.
- [15] B. Elattari and S. A. Gurvitz, Shot noise in coupled dots and the “fractional charges”, *Phys. Lett. A* **292**, 289 (January 2002).
- [16] A. P. Jauho, C. Flindt, T. Novotný, and A. Donarini, Current and current fluctuations in quantum shuttles, *Physics of Fluids* **NN**, xx (November 2005).
- [17] A. N. Jordan and E. V. Sukhorukov, Transport Statistics of Bistable Systems, *Phys. Rev. Lett.* **93**, 260604 (December 2004).
- [18] H. Risken, *The Fokker-Planck Equation*, Springer, Berlin, 1996.